# Quantifying and Controlling Entanglement in the Quantum Magnet Cs$_2$CoCl$_4$

Pontus Laurell [●],[1,2,*] Allen Scheie [●],[3] Chiron J. Mukherjee,[4,5] Michael M. Koza [●],[6] Mechtild Enderle,[6]
Zbigniew Tylczynski,[7] Satoshi Okamoto [●],[8,9] Radu Coldea,[5] D. Alan Tennant [●],[8,9,10,†] and Gonzalo Alvarez[1,2,‡]

[1]*Center for Nanophase Materials Sciences, Oak Ridge National Laboratory, Oak Ridge, Tennessee 37831, USA*
[2]*Computational Science and Engineering Division, Oak Ridge National Laboratory, Oak Ridge, Tennessee 37831, USA*
[3]*Neutron Scattering Division, Oak Ridge National Laboratory, Oak Ridge, Tennessee 37831, USA*
[4]*Science Department, Drew School, San Francisco, California 94115, USA*
[5]*Clarendon Laboratory, Oxford University, Parks Road, Oxford OX1 3PU, United Kingdom*
[6]*Institut Laue-Langevin, 38042 Grenoble Cedex 9, France*
[7]*Faculty of Physics, Adam Mickiewicz University, 61-614 Poznań, Poland*
[8]*Materials Science and Technology Division, Oak Ridge National Laboratory, Oak Ridge, Tennessee 37831, USA*
[9]*Quantum Science Center, Oak Ridge National Laboratory, Oak Ridge, Tennessee 37831, USA*
[10]*Shull-Wollan Center, Oak Ridge National Laboratory, Oak Ridge, Tennessee 37831, USA*

The lack of methods to experimentally detect and quantify entanglement in quantum matter impedes our ability to identify materials hosting highly entangled phases, such as quantum spin liquids. We thus investigate the feasibility of using inelastic neutron scattering (INS) to implement a model-independent measurement protocol for entanglement based on three entanglement witnesses: one-tangle, two-tangle, and quantum Fisher information (QFI). We perform high-resolution INS measurements on Cs$_2$CoCl$_4$, a close realization of the $S = 1/2$ transverse-field $XXZ$ spin chain, where we can control entanglement using the magnetic field, and compare with density-matrix renormalization group calculations for validation. The three witnesses allow us to infer entanglement properties and make deductions about the quantum state in the material. We find QFI to be a particularly robust experimental probe of entanglement, whereas the one and two-tangles require more careful analysis. Our results lay the foundation for a general entanglement detection protocol for quantum spin systems.

*Introduction.*—Quantum entanglement is increasingly considered a vital resource for novel effects and applications [1]. Entanglement is also central to our understanding of many-body systems [2,3], where it forms a deep connection between condensed matter physics and quantum information. Phenomena such as quantum spin liquids [4], topological order [5], quantum criticality [6,7], and thermalization in quantum systems [8] are all inherently related to entanglement properties. It is crucial to develop experimental protocols to detect and quantify entanglement in the solid state, in order to allow unambiguous and rapid identification of quantum materials suitable for new applications and novel insights into complex quantum phenomena.

Because of the rich structure of many-body states, a number of different entanglement measures have been introduced. The most important example in condensed matter theory is entanglement entropy (EE), used to quantify bipartite entanglement. Yet there is no "EE observable" that can be probed directly, which makes experimentally quantifying entanglement in many-body systems challenging [2,9]. Although EE has been measured in cold-atom [10,11] and photonic systems [12], neither

approach is suitable for probing entanglement in macroscopic condensed matter systems.

In special cases, entanglement can be inferred through neutron scattering experiments. For instance, two-spin entanglement within and between dimers [13,14] and entanglement between two molecular magnet qubits [15] have been characterized with neutrons. Also, certain low-dimensional spin systems can be shown to have entanglement via close comparison with theory [16–18]. However, these approaches rely on tractable models, with either small Hilbert spaces or special ground states, which are limited to a handful of systems. For most strongly correlated systems, such methods are not applicable, calling for model-independent approaches.

A promising approach, which we explore in this Letter, is using entanglement witnesses (EWs) [2,3,9], i.e., observables that can be used to identify some *subset* of entangled states. We consider (i) one-tangle ($\tau_1$) [19–21], (ii) concurrence or two-tangle ($\tau_2$) [13,15,19,20,22], and (iii) quantum Fisher information (QFI) [23–25]. These EWs witness (i) entanglement between a spin and the rest of the system, (ii) pairwise entanglement, and (iii) multipartite entanglement, respectively, and thus provide complementary

information. All three EWs are accessible to inelastic neutron scattering (INS) experiments. $\tau_1$ and $\tau_2$ can be obtained from ordered moments and spatial spin-spin correlations [21], whereas QFI can be expressed as an integral of the dynamical spin structure factor (DSF) [25] $S(k, \hbar\omega)$. This powerful formulation of QFI has been applied to experiments on Heisenberg spin chains [26,27], but remains otherwise largely unexplored.

We contrast EE and the mentioned EWs in the spin-1/2 transverse-field $XXZ$ chain. The one-dimensional setting confers an enhanced susceptibility to fluctuations and a higher degree of theoretical tractability, making it an excellent proving ground for our EW protocol. The system hosts two distinct quantum critical points (QCPs) and a classical, minimally entangled point and thus provides a range of interesting behaviors. We study this model numerically using the density-matrix renormalization group (DMRG) [28–30]. We also report high-resolution INS data on the chain compound $Cs_2CoCl_4$, known to be an excellent realization of the $XXZ$ model [31–37]. We find that QFI values extracted from experiment and simulation show good agreement, demonstrating it is an experimentally viable probe of entanglement. We also find the experimental one-tangle to deviate from theory in a potentially revealing manner, whereas the two-tangle extraction requires spin-polarization-resolved experiments.

*Transverse-field XXZ chain.*—A particularly rich yet simple system is found in the $XXZ$ chain,

$$H = \sum_{i=1}^{L}[J(S_i^x S_{i+1}^x + S_i^y S_{i+1}^y + \Delta S_i^z S_{i+1}^z) + h_x S_i^x], \quad (1)$$

where $S_i^\alpha$, $\alpha \in \{x, y, z\}$, are spin-1/2 operators, $\Delta$ represents exchange anisotropy, and $h_x$ is a uniform magnetic field in the transverse ($\hat{x}$) direction. For $Cs_2CoCl_4$ we take the parameters $J = 0.23$ meV and $\Delta = 0.25$ [34], but we note $\Delta \approx 0.12$ has been proposed elsewhere [36,37]. (We consider other $\Delta$ values in the Supplemental Material [38].) The model is also relevant to quantum simulation using cold atoms in optical lattices [46].

For $h_x = 0$, the model can be solved exactly using the Bethe ansatz [47–49]. However, a finite transverse field breaks integrability and induces a new source of fluctuations when $\Delta \neq 1$. The model is particularly nontrivial in the spin-flop region, $-1 < \Delta < 1$ [50], where its phase diagram contains two QCPs, as shown in Fig. 1(a). At the first QCP, $h_x = 0$, it is equivalent to a gapless Luttinger liquid, which is described by a conformal field theory (CFT) with central charge $c = 1$ [6]. At $h_x > 0$, a gapped, long-range Néel order develops, with a staggered magnetization component $m_{st}^y$ along $\hat{y}$ and a magnetization component $m^x$ along $\hat{x}$ [38]. This order remains up to a critical field $h_c$, where the system is described by a $c = 1/2$ CFT. Above $h_c$ a gapped, nondegenerate spin-polarized (paramagnetic) phase develops and $m^x$ saturates asymptotically. There also exists a "classical" or factoring field
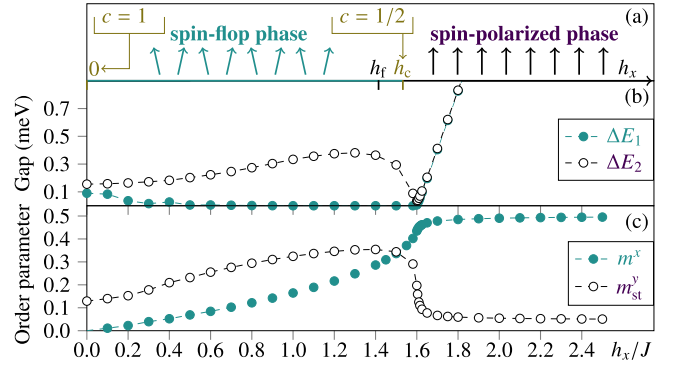


FIG. 1. (a) Schematic phase diagram for $-1 \leq \Delta \leq 1$. There are two quantum critical points at $h_x = 0$ and $h_c$, and a classical point at a factoring field $h_f$, close to $h_c$. For $\Delta = 0.25$, $h_f \approx 1.58J$ and $h_c \approx 1.6J$. The distance $h_c - h_f$ is exaggerated for clarity. (b) Energy gap and (c) magnetization and staggered magnetization [38] from DMRG for $\Delta = 0.25$, $J = 0.23$ meV. Nonvanishing $\Delta E_i$, $m_{st}^y$ at $h_x = 0$, and $m_{st}^y \neq 0$ at $h_x \geq h_c$, are due to a finite-size effect in the DMRG calculation.

$h_f(\Delta) = J\sqrt{2(1 + \Delta)}$, where the ground state is exactly of the classical spin-flop Néel type [51,52]. At $h_f$, quantum fluctuations are precisely balanced by the field, and entanglement estimators indicate an entanglement transition [21,53–55].

The model has previously been studied using Jordan-Wigner fermion mean-field theory [50,56], exact diagonalization [57], DMRG [56,58,59], and quantum Monte Carlo methods [21]. The real-frequency dynamics were studied in Refs. [56,59], where the mean-field theory [56] was found to give qualitatively different spectra to the DMRG calculation [59] at $h_x \leq h_c$. Here we use a $T = 0$ DMRG method described in the Supplemental Material [38]. Care is taken to relate our finite-size ($L = 100$ unless stated otherwise) results in the spin-flop region to the thermodynamic limit [38,56,59]. There is a finite-size gap between a unique ground state and the first excited state, $\Delta E_1 = E_1 - E_0$, where $E_n$ is the energy of the $n$th state. The physical excitation gap is given instead by $\Delta E_2 = E_2 - E_0 > \Delta E_1$, as shown in Fig. 1(b). Magnetization is plotted in Fig. 1(c).

*Experimental method.*—INS data on a high-quality 9 g solution-grown $Cs_2CoCl_4$ single crystal were collected using the direct-geometry time-of-flight spectrometer IN6 at Institut Laue-Langevin, with monochromatic incident neutrons of 2.35 meV. Cooling was provided by a dilution refrigerator, and data were collected at 70 mK ($\approx 0.026J \approx 6\ \mu eV$). The sample was oriented with crystallographic $b$, $c$ axes in the horizontal scattering plane. Magnetic fields up to 2.5 T were applied along the $a$ axis using a vertical field cryomagnet. For more details about the experiments, see Ref. [60]. Raw neutron counts were normalized by the integrated quasielastic incoherent scattering to account in a first approximation for neutron

absorption from the sample. The nonmagnetic background was modeled and subtracted, and resulting counts were divided by the squared spherical magnetic form factor for $Co^{2+}$, so resulting intensities are proportional to the purely magnetic scattering cross section.

The $Co^{2+}$ ions in $Cs_2CoCl_4$ form a Kramers doublet, which can be described by an effective spin $S = 1/2$. Magnetic interactions between $Co^{2+}$ ions are quasi-1D along the $b$ axis, with exchange interaction much lower than the energy gap to higher crystal field levels, resulting in an effective spin-1/2 Hamiltonian with strong $XXZ$ anisotropy. Finite 3D interchain couplings (estimated to be at least an order of magnitude smaller than $J$ [33,37,61,62]) stabilize long-range order below $T_N = 0.212$ K with ordering wave vector $q = (0, 1/2, 1/2)$, where spins point near the $b$ axis. Transverse magnetic fields applied along the $a$ axis suppress this order at $h_c^{exp} = 2.10(4)$ T [34]. This field direction is at an $\approx 40°$ angle to the $xy$ easy plane of the spins. This angle—along with interchain couplings [62,63]—is expected to renormalize transition fields compared to the in plane field case considered in Eq. (1), but not to change the qualitative content of the phase diagram. To compare experimental and DMRG results, we scale fields such that $h_c^{DMRG} \approx 1.604J = h_c^{exp}$.

*Spectra.*—Figure 2 compares INS spectra for $Cs_2CoCl_4$ with spectra calculated for Eq. (1). For more field strengths

and processing details, see the Supplemental Material [38]. At low fields, the data qualitatively agree with simulations of the ideal chain model, Eq. (1). Interchain couplings become qualitatively important near $h_c$, where the field-dependent gap is of similar strength to the interchain exchange. Interchain couplings also produce a band splitting at high fields, as seen in Figs. 2(j) and 2(k), whereas the DMRG spectrum reduces to a single magnon branch. Hence, we conclude that $Cs_2CoCl_4$ is 1D-like for weak and intermediate fields. Precise modeling of interchain effects is beyond the scope of this work.

At zero field, the main contributions to the DSF come from the two-spinon continuum [64,65], bounds of which are drawn in Figs. 2(a) and 2(b). At finite field, the excitation branches begin to split [Figs. 2(d) and 2(e)], eventually decoupling the upper branch from the low-energy excitations, forming a high-energy feature at $\hbar\omega \geq 0.4$ meV. As Ref. [59] noted, this feature is beyond the mean-field prediction [56]. Here we see it is present in the experimental material [Figs. 2(d) and 2(g)] and DMRG [Figs. 2(e) and 2(h)]. The intensity of this high-energy feature weakens as $h_c$ is approached from below, and as Figs. 2(j) and 2(k) show, it disappears above $h_c$. To understand its origin, it is instructive to consider the factoring field. While the ground state at $h_f$ is classical, the dynamics cannot be fully described using linear spin wave theory (LSWT) [52,66]. For Eq. (1), the dynamics is LSWT-like only near $k = \pi$ for $S^{xx}(k, \hbar\omega)$ and near $k = 0$ for $S^{yy/zz}(k, \hbar\omega)$ [52]. As Fig. 3 shows, this behavior agrees well with DMRG. The high-energy feature vanishes at $k$ points where LSWT is exact, heavily suggesting its origin is in multimagnon physics, as proposed in Ref. [59].

*Entanglement.*—We now investigate the quantum phase transition (QPT) of Eq. (1) and $Cs_2CoCl_4$ using entanglement measures. Figure 4(a) shows half-chain von Neumann EE. At QCPs, in a system of length $L$ with open boundaries, it is expected to follow the CFT expression [7]
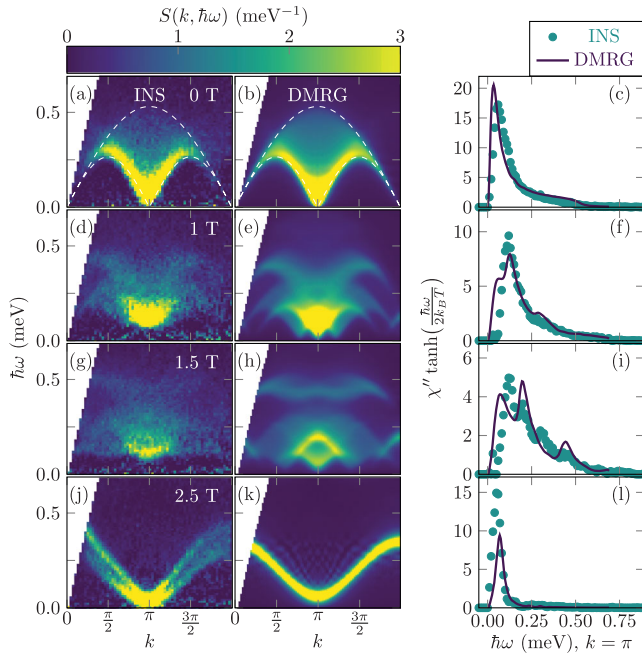


FIG. 2. (a),(d),(g),(j) INS spectra for $Cs_2CoCl_4$ at four representative field strengths. (b),(e),(h),(k) Calculated spectra for the $XXZ$ chain at matching fields, accounting for the experimental polarization factor. (c),(f),(i),(l) QFI integrand at $k = \pi$. White dashed lines in (a) and (b) bound the two-spinon continua. Throughout we designate the wave vector component $k$ along the chain in units of $1/b$.
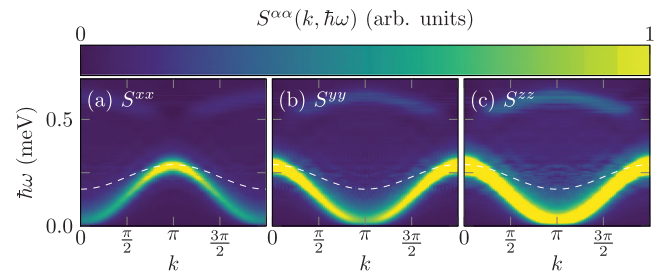


FIG. 3. Theoretical DSF for $J = 0.23$ meV, $\Delta = 0.25$, and $h_x = 1.58114J \approx 2.07T \approx h_f$. Dashed white lines show linear spin wave energy predictions [52]. Agreement with DMRG is excellent at $k = \pi$ in (a) and $k = 0$ in (b),(c). Elsewhere in the Brillouin zone, the dispersion is significantly modified by anharmonic terms in the full spin wave Hamiltonian. Note that the experimental polarization factor has not been applied [see [38], Eq. (S5)].
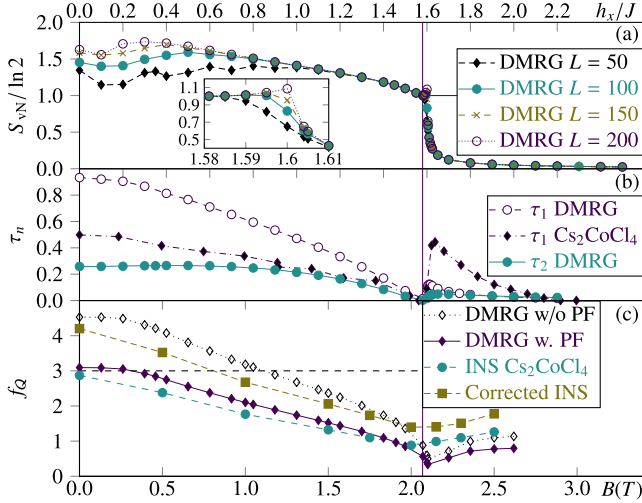
FIG. 4. (a) Entanglement entropy $S_{vN}$ from DMRG as a function of $h_x$. The vertical line indicates the factoring field, where $S_{vN} \approx \ln 2$ (horizontal line). For $h_x > h_c$ there is a steep drop in entropy as the system enters a polarized phase with a nondegenerate ground state. Inset: EE near $h_c$. (b) The approximate one-($\tau_1$) and two-tangles ($\tau_2$) reach a minimum at $h_f$. (c) QFI from INS and DMRG $S(k, \hbar\omega)$. Above the horizontal dashed line, QFI indicates the presence of *at least* bipartite entanglement. Below it, QFI cannot be used to distinguish separable and entangled states. The PF-corrected INS $f_Q$ line is obtained by scaling $f_Q^{\text{INS}}$ by the ratio between the two DMRG $f_Q$ values [38].

$S_{vN} = (c/6) \ln[L/\pi] + C$, where $C$ is a nonuniversal correction. We observe approximately logarithmic scaling at the QCPs and saturation of $S_{vN}$ for most noncritical fields [6]. Notably, we find at $h_f$ that $S_{vN} = \ln 2$ to good approximation, consistent with a twofold classical ground-state degeneracy.

Another sharp signature of the classical state has previously been found using entanglement estimators [21,54,55]. We consider one-tangle $\tau_1$, which quantifies entanglement between a single site and the rest of the system, and two-tangle $\tau_2$, which quantifies the total pairwise entanglement in the system and satisfies $\tau_2 < \tau_1$ [19,67]. For translation-invariant $S = 1/2$ systems, $\tau_1$ can be defined in terms of spin expectation values at a given site $j$, $\tau_1 = 1 - 4\sum_\alpha (\langle S_j^\alpha \rangle)^2$. It is useful for interpreting experiments, with the caveat that it is only strictly defined at $T = 0$. We approximate $\tau_1$ by keeping only ferro- and antiferromagnetic ordered moments [38]. The theoretical prediction is shown in Fig. 4(b), along with experimental results obtained [38] using 80 mK ($\approx 0.03J$) data from Ref. [34]. At zero field, the experimental $\tau_1$ is reduced from the theoretical value due to magnetic ordering at low temperature, but still indicates substantial entanglement. We discuss the high $\tau_1$ at $B > 2$ T later.

Next, two-tangle is defined as $\tau_2 = 2\sum_{r \neq 0} C_r^2$, where $C_r$ is the concurrence for separation $r$. $C_r$ for the $S =$

$1/2$ *XXZ* model absent spontaneous symmetry breaking ($m_{\text{st}}^y = 0$) can be defined [20–22,53] $C_r = 2\max\{0, C_r', C_r''\}$, where

$$C_r' = |\langle S_i^y S_{i+r}^y \rangle + \langle S_i^z S_{i+r}^z \rangle| - \sqrt{\left(\frac{1}{4} + \langle S_i^x S_{i+r}^x \rangle\right)^2 - (m^x)^2},$$

(2)

$$C_r'' = \langle S_i^x S_{i+r}^x \rangle + |\langle S_i^y S_{i+r}^y \rangle - \langle S_i^z S_{i+r}^z \rangle| - \frac{1}{4}.$$ (3)

This definition acts as a lower bound for pairwise entanglement in the symmetry-broken state [68,69]. While such correlation functions are straightforward to compute theoretically, for anisotropic systems they require spin-polarization-resolved techniques to measure experimentally. Since we have not conducted such experiments, we plot only the theoretical $\tau_2$ in Fig. 4(b). (In the Supplemental Material [38], we simulate a polarized INS experiment by using DMRG to correct for polarization factors (PFs) and estimate concurrence and $\tau_2$ from unpolarized data. We find rough agreement between experiment and theory at low fields, suggesting $\tau_2$ could be a reliable EW with carefully performed experiments.)

Finally, we come to the quantum Fisher information. The QFI density $f_Q$ can be expressed as [25]

$$f_Q(k, T) = \frac{4}{\pi} \int_0^\infty d(\hbar\omega) \tanh\left(\frac{\hbar\omega}{2k_B T}\right) \chi''(k, \hbar\omega, T),$$ (4)

where the dynamical susceptibility $\chi''$ is linked to the DSF through the fluctuation-dissipation theorem $\chi''(k, \hbar\omega, T) = \tanh(\hbar\omega/2k_B T)S(k, \hbar\omega)$, and $S(k, \hbar\omega)$ is normalized per site (i.e., intensive) according to the sum rule $\sum_{\alpha \in \{x,y,z\}} \int_{-\infty}^\infty d(\hbar\omega) \int_0^{2\pi} dk S^{\alpha\alpha}(k, \hbar\omega) = S(S+1)$. We are interested in $f_Q(k = \pi)$, which witnesses entanglement associated with the antiferromagnetic ordering [38]. Importantly, one can derive bounds for $f_Q$ that can only be met by certain classes of entangled states [70–72]. For unpolarized neutron scattering and $S = 1/2$ systems, $f_Q > 3n$, with $n$ a divisor of $L$, indicates the system is at least $n + 1$-partite entangled [38].

Figure 4(c) shows QFI determined from INS data normalized against DMRG [38], and from DMRG with and without PF applied. All QFI integrals used $T = 70$ mK. In all cases, maximal $f_Q$ occurs at $h_x = 0$. Unlike $\tau_1$, QFI is insensitive to zero-field magnetic order since elastic peaks are suppressed by the tanh factor in Eq. (4). The results indicate the experimental PF suppresses QFI below the lower bound required to observe bipartite entanglement. Using DMRG intensities, we can obtain PF-corrected values [38], which do witness at least bipartite entanglement at the lowest measured fields. This finding highlights that it is easy to underestimate the underlying QFI due to resolution effects and calls for higher resolution in future experiments.

Additionally, it would be valuable to derive tighter bounds on $f_Q$, even if they do not apply in general [73,74].

There is qualitative and reasonably quantitative agreement between DMRG and INS QFI at intermediate fields ($\lesssim 1.75$ T), but not at high fields, where interchain coupling causes deviations from ideal 1D behavior. In particular, interchain coupling raises the field required for full polarization, which may explain the observed increase in $f_Q$ above $h_c$. As $h_x \to \infty$ we expect $f_Q$ to vanish. In addition, the $f_Q^{DMRG}$ minimum occurs at $h_c$, while the $f_Q^{INS}$ minimum appears at a lower field, likely due to deviations from ideal 1D behavior.

Another deviation from 1D behavior is seen in the large $\tau_1$ at $B > 2$ T [Fig. 4(b)], which could naively be interpreted as a sign that the system has entered a highly entangled state. However, this scenario seems unlikely given the observed $f_Q$ behavior and suppression of magnetic fluctuations at high field. Instead, $\tau_1$ is likely overestimated in this region due to spin correlations not captured by the ferro- and antiferromagnetic ordered moments used to evaluate $\tau_1$, induced by the small but finite interchain couplings, which become relevant for fields near $h_c$, where the spin gap is small and the system is near critical. Capturing such 3D effects is beyond the scope of the current Letter.

On its face, the low $f_Q$ values at $h_c$ may seem incompatible with the prediction that CFTs have both large bipartite and multipartite entanglement [75]. QFI near $h_c$ is low because the Néel order parameter becomes vanishingly small near the transition to the polarized state, such that there is little spectral weight available for entanglement [76], and so $f_Q(k = \pi)$ is not an effective witness at this QCP. We generically expect QFI associated with antiferromagnetic ordering vectors to demonstrate significant entanglement only away from paramagnetic transitions. This illustrates a general limitation of EWs: they are not universal [9]. Thus additional EWs would be required to experimentally characterize the entanglement properties of the transverse-field *XXZ* chain in the entire field range.

*Conclusion.*—We have contrasted several entanglement measures by applying them to $Cs_2CoCl_4$ and the transverse-field *XXZ* chain. Although we are unable to directly witness genuine multipartite entanglement in $Cs_2CoCl_4$, the strong agreement between DMRG and INS QFI suggests QFI is already a useful tool for qualitative investigations of entanglement properties, potentially even for topological phases [77–79]. With improved resolution and bounds it can also prove valuable for directly quantifying *local* entanglement in materials. QFI can be used in combination with other EWs, to infer entanglement properties as a control parameter is tuned. Such combinations may be required since paramagnetic QPTs remain inaccessible to $f_Q(k = \pi)$. We find both one-tangle and QFI to be useful measures for inelastic experiments in general, whereas two-tangle requires polarization analysis. We expect the model-independent approach we outline here, which applies to many spectroscopic techniques and also to higher-dimensional systems, will prove useful in identifying materials with entangled states and highly quantum properties. As the search for materials realizing exotic quantum states continues, EWs can allow clear discrimination between truly entangled and disordered nonentangled states.

Access to the data reported in this paper will be made available from Ref. [80].

[*]laurell@utexas.edu
[†]tennantda@ornl.gov
[‡]alvarezcampg@ornl.gov

[1] R. Horodecki, P. Horodecki, M. Horodecki, and K. Horodecki, Quantum entanglement, Rev. Mod. Phys. **81**, 865 (2009).

[2] L. Amico, R. Fazio, A. Osterloh, and V. Vedral, Entanglement in many-body systems, Rev. Mod. Phys. **80**, 517 (2008).

[3] V. Vedral, Quantifying entanglement in macroscopic systems, Nature (London) **453**, 1004 (2008).

[4] L. Savary and L. Balents, Quantum spin liquids: A review, Rep. Prog. Phys. **80**, 016502 (2017).

[5] X.-G. Wen, Colloquium: Zoo of quantum-topological phases of matter, Rev. Mod. Phys. **89**, 041004 (2017).

[6] G. Vidal, J. I. Latorre, E. Rico, and A. Kitaev, Entanglement in Quantum Critical Phenomena, Phys. Rev. Lett. **90**, 227902 (2003).

[7] P. Calabrese and J. Cardy, Entanglement entropy and quantum field theory, J. Stat. Mech. (2004) P06002.

[8] D. A. Abanin, E. Altman, I. Bloch, and M. Serbyn, Colloquium: Many-body localization, thermalization, and entanglement, Rev. Mod. Phys. **91**, 021001 (2019).

[9] O. Gühne and G. Tóth, Entanglement detection, Phys. Rep. **474**, 1 (2009).

[10] R. Islam, R. Ma, P. M. Preiss, M. E. Tai, A. Lukin, M. Rispoli, and M. Greiner, Measuring entanglement entropy in a quantum many-body system, Nature (London) **528**, 77 (2015).

[11] A. M. Kaufman, M. E. Tai, A. Lukin, M. Rispoli, R. Schittko, P. M. Preiss, and M. Greiner, Quantum

thermalization through entanglement in an isolated many-body system, Science **353,** 794 (2016).

[12] I. Pitsios, leonardo Banchi, A. S. Rab, M. Bentivegna, D. Caprara, A. Crespi, N. Spagnolo, S. Bose, P. Mataloni, R. Osellame, and F. Sciarrino, Photonic simulation of entanglement growth and engineering after a spin chain quench, Nat. Commun. **8,** 1569 (2017).

[13] Č. Brukner, V. Vedral, and A. Zeilinger, Crucial role of quantum entanglement in bulk properties of solids, Phys. Rev. A **73,** 012110 (2006).

[14] D. A. Tennant, C. Broholm, D. H. Reich, S. E. Nagler, G. E. Granroth, T. Barnes, K. Damle, G. Xu, Y. Chen, and B. C. Sales, Neutron scattering study of two-magnon states in the quantum magnet copper nitrate, Phys. Rev. B **67,** 054414 (2003).

[15] E. Garlatti, T. Guidi, S. Ansbro, P. Santini, G. Amoretti, J. Ollivier, H. Mutka, G. Timco, I. J. Vitorica-Yrezabal, G. F. S. Whitehead, R. E. P. Winpenny, and S. Carretta, Portraying entanglement between molecular qubits with four-dimensional inelastic neutron scattering, Nat. Commun. **8,** 14543 (2017).

[16] M. Mourigal, M. Enderle, A. Klöpperpieper, J.-S. Caux, A. Stunault, and H. M. Rønnow, Fractional spinon excitations in the quantum Heisenberg antiferromagnetic chain, Nat. Phys. **9,** 435 (2013).

[17] B. D. Piazza, M. Mourigal, N. B. Christensen, G. J. Nilsen, P. Tregenna-Piggott, T. G. Perring, M. Enderle, D. F. McMorrow, D. A. Ivanov, and H. M. Rønnow, Fractional excitations in the square-lattice quantum antiferromagnet, Nat. Phys. **11,** 62 (2015).

[18] N. B. Christensen, H. M. Rønnow, D. F. McMorrow, A. Harrison, T. G. Perring, M. Enderle, R. Coldea, L. P. Regnault, and G. Aeppli, Quantum dynamics and entanglement of spins on a square lattice, Proc. Natl. Acad. Sci. U.S.A. **104,** 15264 (2007).

[19] V. Coffman, J. Kundu, and W. K. Wootters, Distributed entanglement, Phys. Rev. A **61,** 052306 (2000).

[20] L. Amico, A. Osterloh, F. Plastina, R. Fazio, and G. Massimo Palma, Dynamics of entanglement in one-dimensional spin systems, Phys. Rev. A **69,** 022304 (2004).

[21] T. Roscilde, P. Verrucchi, A. Fubini, S. Haas, and V. Tognetti, Studying Quantum Spin Systems through Entanglement Estimators, Phys. Rev. Lett. **93,** 167203 (2004).

[22] L. Amico, F. Baroni, A. Fubini, D. Patanè, V. Tognetti, and P. Verrucchi, Divergence of the entanglement range in low-dimensional quantum systems, Phys. Rev. A **74,** 022322 (2006).

[23] L. Pezzé and A. Smerzi, Entanglement, Nonlinear Dynamics, and the Heisenberg Limit, Phys. Rev. Lett. **102,** 100401 (2009).

[24] H. Strobel, W. Muessel, D. Linnemann, T. Zibold, D. B. Hume, L. Pezzè, A. Smerzi, and M. K. Oberthaler, Fisher information and entanglement of non-Gaussian spin states, Science **345,** 424 (2014).

[25] P. Hauke, M. Heyl, L. Tagliacozzo, and P. Zoller, Measuring multipartite entanglement through dynamic susceptibilities, Nat. Phys. **12,** 778 (2016).

[26] G. Mathew, S. L. L. Silva, A. Jain, A. Mohan, D. T. Adroja, V. G. Sakai, C. V. Tomy, A. Banerjee, R. Goreti, Aswathi V. N., R. Singh, and D. Jaiswal-Nagar, Experimental

[27] A. Scheie, P. Laurell, A. M. Samarakoon, B. Lake, S. E. Nagler, G. E. Granroth, S. Okamoto, G. Alvarez, and D. A. Tennant, Witnessing entanglement in quantum magnets using neutron scattering, Phys. Rev. B **103,** 224434 (2021).

[28] S. R. White, Density Matrix Formulation for Quantum Renormalization Groups, Phys. Rev. Lett. **69,** 2863 (1992).

[29] S. R. White, Density-matrix algorithms for quantum renormalization groups, Phys. Rev. B **48,** 10345 (1993).

[30] G. Alvarez, The density matrix renormalization group for strongly correlated electron systems: A generic implementation, Comput. Phys. Commun. **180,** 1572 (2009).

[31] H. Algra, L. de Jongh, H. Blte, W. Huiskamp, and R. Carlin, Heat capacity of $Cs_2CoCl_4$ below 1 K, compared with the $S = \frac{1}{2}$ linear chain $XY$ model, Physica (Amsterdam) **82B+C,** 239 (1976).

[32] J. N. McElearney, S. Merchant, G. E. Shankle, and R. L. Carlin, Low-temperature magnetic characteristics of tetrahedral $CoCl_4^{2-}$. III. Magnetic exchange in paramagnetic $Cs_2CoCl_4$, J. Chem. Phys. **66,** 450 (1977).

[33] H. Yoshizawa, G. Shirane, H. Shiba, and K. Hirakawa, Neutron scattering study of a one-dimensional $XY$ antiferromagnet $Cs_2CoCl_4$, Phys. Rev. B **28,** 3904 (1983).

[34] M. Kenzelmann, R. Coldea, D. A. Tennant, D. Visser, M. Hofmann, P. Smeibidl, and Z. Tylczynski, Order-to-disorder transition in the $XY$-like quantum magnet $Cs_2CoCl_4$ induced by noncommuting applied fields, Phys. Rev. B **65,** 144432 (2002).

[35] C. Mukherjee, R. Coldea, D. Tennant, M. Koza, M. Enderle, K. Habicht, P. Smeibidl, and Z. Tylczynski, Field-induced quantum phase transition in the quasi 1D $XY$-like antiferromagnet $Cs_2CoCl_4$, J. Magn. Magn. Mater. **272–276,** 920 (2004).

[36] O. Breunig, M. Garst, E. Sela, B. Buldmann, P. Becker, L. Bohatý, R. Müller, and T. Lorenz, Spin-$\frac{1}{2}$ $XXZ$ Chain System $Cs_2CoCl_4$ in a Transverse Magnetic Field, Phys. Rev. Lett. **111,** 187202 (2013).

[37] O. Breunig, M. Garst, A. Rosch, E. Sela, B. Buldmann, P. Becker, L. Bohatý, R. Müller, and T. Lorenz, Low-temperature ordered phases of the spin-$\frac{1}{2}$ $XXZ$ chain system $Cs_2CoCl_4$, Phys. Rev. B **91,** 024423 (2015).

[38] See Supplemental Material at http://link.aps.org/supplemental/10.1103/PhysRevLett.127.037201, which includes Refs. [39–45], for detailed methods, supplemental results, and useful analytical results on the 1D model.

[39] T. D. Kühner and S. R. White, Dynamical correlation functions using the density matrix renormalization group, Phys. Rev. B **60,** 335 (1999).

[40] A. Nocera and G. Alvarez, Spectral functions with the density matrix renormalization group: Krylov-space approach for correction vectors, Phys. Rev. E **94,** 053308 (2016).

[41] E. Jeckelmann, Dynamical density-matrix renormalization-group method, Phys. Rev. B **66,** 045114 (2002).

[42] K. Fabricius, U. Löw, and J. Stolze, Dynamic correlations of antiferromagnetic spin-$\frac{1}{2}$ $XXZ$ chains at arbitrary temperature from complete diagonalization, Phys. Rev. B **55,** 5833 (1997).

[43] C. N. Yang and C. P. Yang, Ground-state energy of a Heisenberg-Ising lattice, Phys. Rev. **147**, 303 (1966).

[44] E. Lieb and D. Mattis, Ordering energy levels of interacting spin systems, J. Math. Phys. (N.Y.) **3**, 749 (1962).

[45] I. Affleck and E. Lieb, A proof of part of Haldane's conjecture on spin chains, Lett. Math. Phys. **12**, 57 (1986).

[46] T. L. Nguyen, J. M. Raimond, C. Sayrin, R. Cortiñas, T. Cantat-Moltrecht, F. Assemat, I. Dotsenko, S. Gleyzes, S. Haroche, G. Roux, T. Jolicoeur, and M. Brune, Towards Quantum Simulation with Circular Rydberg Atoms, Phys. Rev. X **8**, 011032 (2018).

[47] C. N. Yang and C. P. Yang, One-dimensional chain of anisotropic spin-spin interactions. I. Proof of Bethe's hypothesis for ground state in a finite system, Phys. Rev. **150**, 321 (1966).

[48] C. N. Yang and C. P. Yang, One-dimensional chain of anisotropic spin-spin interactions. II. Properties of the ground-state energy per lattice site for an infinite system, Phys. Rev. **150**, 327 (1966).

[49] J. des Cloizeaux and M. Gaudin, Anisotropic linear magnetic chain, J. Math. Phys. (N.Y.) **7**, 1384 (1966).

[50] D. V. Dmitriev, V. Y. Krivnov, A. A. Ovchinnikov, and A. Langari, One-dimensional anisotropic Heisenberg model in the transverse magnetic field, JETP **95**, 538 (2002).

[51] J. Kurmann, H. Thomas, and G. Müller, Antiferromagnetic long-range order in the anisotropic quantum spin chain, Physica (Amsterdam) **112A**, 235 (1982).

[52] G. Müller and R. E. Shrock, Implications of direct-product ground states in the one-dimensional quantum $XYZ$ and $XY$ spin chains, Phys. Rev. B **32**, 5845 (1985).

[53] J. Abouie, A. Langari, and M. Siahatgar, Thermodynamic behavior of the $XXZ$ Heisenberg $s = 1/2$ chain around the factorizing magnetic field, J. Phys. Condens. Matter **22**, 216008 (2010).

[54] L. Amico, D. Rossini, A. Hamma, and V. E. Korepin, Optimal Correlations in Many-Body Quantum Systems, Phys. Rev. Lett. **108**, 240503 (2012).

[55] S. Mahdavifar, S. Mahdavifar, and R. Jafari, Magnetic quantum correlations in the one-dimensional transverse-field $XXZ$ model, Phys. Rev. A **96**, 052303 (2017).

[56] J.-S. Caux, F. H. L. Essler, and U. Löw, Dynamical structure factor of the anisotropic Heisenberg chain in a transverse field, Phys. Rev. B **68**, 134431 (2003).

[57] A. Langari and S. Mahdavifar, Gap exponent of the $XXZ$ model in a transverse field, Phys. Rev. B **73**, 054410 (2006).

[58] F. Capraro and C. Gros, The spin-1/2 anisotropic Heisenberg-chain in longitudinal and transversal magnetic fields: A DMRG study, Eur. Phys. J. B **29**, 35 (2002).

[59] B. Bruognolo, A. Weichselbaum, J. von Delft, and M. Garst, Dynamic structure factor of the spin-$\frac{1}{2}$ $XXZ$ chain in a transverse field, Phys. Rev. B **94**, 085136 (2016).

[60] C. Mukherjee, Neutron scattering studies on low-dimensional quantum magnets, Ph.D. thesis, University of Oxford, 2005.

[61] I. Chatterjee, Order–disorder transition in one-dimensional quantum magnet, J. Magn. Magn. Mater. **265**, 363 (2003).

[62] D. V. Dmitriev and V. Y. Krivnov, Quasi-one-dimensional anisotropic Heisenberg model in a transverse magnetic field, JETP Lett. **80**, 303 (2004).

[63] D. V. Dmitriev and V. Y. Krivnov, Anisotropic Heisenberg chain in coexisting transverse and longitudinal magnetic fields, Phys. Rev. B **70**, 144414 (2004).

[64] G. Müller, H. Thomas, M. W. Puga, and H. Beck, Quantum spin dynamics of the one-dimensional planar antiferromagnet, J. Phys. C **14**, 3399 (1981).

[65] J.-S. Caux and J. M. Maillet, Computation of Dynamical Correlation Functions of Heisenberg Chains in a Magnetic Field, Phys. Rev. Lett. **95**, 077201 (2005).

[66] J. H. Taylor and G. Müller, Limitations of spin-wave theory in $T = 0$ spin dynamics, Phys. Rev. B **28**, 1529 (1983).

[67] T. J. Osborne and F. Verstraete, General Monogamy Inequality for Bipartite Qubit Entanglement, Phys. Rev. Lett. **96**, 220503 (2006).

[68] O. F. Syljuåsen, Entanglement and spontaneous symmetry breaking in quantum spin models, Phys. Rev. A **68**, 060301 (R) (2003).

[69] A. Osterloh, G. Palacios, and S. Montangero, Enhancement of Pairwise Entanglement via $\mathbb{Z}_2$ Symmetry Breaking, Phys. Rev. Lett. **97**, 257201 (2006).

[70] P. Hyllus, W. Laskowski, R. Krischek, C. Schwemmer, W. Wieczorek, H. Weinfurter, L. Pezzé, and A. Smerzi, Fisher information and multiparticle entanglement, Phys. Rev. A **85**, 022321 (2012).

[71] G. Tóth, Multipartite entanglement and high-precision metrology, Phys. Rev. A **85**, 022322 (2012).

[72] L. Pezzè and A. Smerzi, *Atom Interferometry, Proceedings of the International School of Physics Enrico Fermi, Course 188, Varenna* (IOS Press, Amsterdam, 2014), Chap. Quantum theory of phase estimation, pp. 691–741.

[73] I. Apellaniz, M. Kleinmann, O. Gühne, and G. Tóth, Optimal witnessing of the quantum Fisher information with few measurements, Phys. Rev. A **95**, 032330 (2017).

[74] R. C. de Almeida and P. Hauke, From entanglement certification with quench dynamics to multipartite entanglement of interacting fermions, arXiv:2005.03049.

[75] M. A. Rajabpour, Multipartite entanglement and quantum Fisher information in conformal field theories, Phys. Rev. D **96**, 126007 (2017).

[76] N. Blanc, J. Trinh, L. Dong, X. Bai, A. A. Aczel, M. Mourigal, L. Balents, T. Siegrist, and A. P. Ramirez, Quantum criticality among entangled spin chains, Nat. Phys. **14**, 273 (2018).

[77] L. Pezzè, M. Gabbrielli, L. Lepori, and A. Smerzi, Multipartite Entanglement in Topological Quantum Phases, Phys. Rev. Lett. **119**, 250401 (2017).

[78] M. Gabbrielli, A. Smerzi, and L. Pezzè, Multipartite entanglement at finite temperature, Sci. Rep. **8**, 15663 (2018).

[79] J. Lambert and E. S. Sørensen, Revealing divergent length scales using quantum Fisher information in the Kitaev honeycomb model, Phys. Rev. B **102**, 224401 (2020).

[80] P. Laurell, A. Scheie, C. J. Mukherjee, M. M. Koza, M. Enderle, Z. Tylczynski, S. Okamoto, R. Coldea, D. A. Tennant, and G. Alvarez, Quantifying and Controlling Entanglement in the Quantum Magnet $Cs_2CoCl_4$ (University of Oxford, Oxford, 2021), https://doi.org/10.5287/bodleian:j0z4nb9eq.